Water/magma interaction:
some theory and experiments on peperite formation

Kenneth Wohletz

Los Alamos National Laboratory, Earth and Environmental Sciences Division, Los Alamos, NM 87545, USA

Abstract

Experiments, using molten thermite as a magma analog, produce peperite when the melt interacts with wet sand. These experiments also show explosive behavior, developing Strombolian- and Surtseyan-like bursts. The results demonstrate that the application of fuel–coolant interaction (FCI) theory is appropriate for interpretation of peperites. The theory described includes discussion of the importance of mass interaction ratios of wet sediment and magma (R_s), which determine thermal equilibrium temperature limits and contact interface dynamics. The dynamics of the interface between magma and wet sediments involves heat transfer over a wide range of rates from passive quenching to explosive fragmentation. A vapor film layer develops at the interface and acts both as an insulating barrier, promoting passive quenching, as well as a potential energy reservoir that can cause magma fragmentation, mingling of the magma with wet sediments, and explosive quenching when the vapor film becomes unstable. An important parameter in determining the behavior of the vapor film is the value of R_s, which controls whether heat can be convectively removed from the layer as more is being added from its contact with magma. If $R_s > 1$ for fully saturated sediments, there is enough water in the sediments to make convective heat flow effective in quenching the magma, but below that value, there is the potential that the vapor film will be unstable, producing highly dynamic phenomena, including explosive fragmentation. At values of $R_s < 0.1$ there is insufficient water to allow the escalation of explosive fragmentation. © 2002 Elsevier Science B.V. All rights reserved.

Keywords: peperite; hydrovolcanism; fragmentation; explosion phenomena; experiments; fuel–coolant interaction

1. Introduction

Experimental volcanology at Los Alamos National Laboratory first began in 1975 under the direction of Thomas McGetchin. I followed a twin approach of exploring both novel computer simulations and scaled model volcano experiments. The scaled models provided an experimental basis for analyzing and adapting the numerical simulations. These experiments simulated both effusive and explosive eruption physics. The early models (McGetchin et al., 1976; Widdicombe et al., 1976) employed Carbowax™ as a lava analog for effusive eruptions. This polymer forms a two-phase (liquid and solid) system at temperatures near 40°C and can develop flows comparable to those of lava while satisfying most criteria of similitude. In later experiments Wohletz and McQueen (1984) and Wohletz et al. (1995) uti-

E-mail address: wohletz@lanl.gov (K. Wohletz).

lized molten thermite as a magma analog for producing gas-rich explosions by interaction with external water. We chose thermite because large batches of melt can be generated easily by its exothermic reaction. Its physical and chemical properties are also well suited for a basalt analog. The thermite experiments continued periodically over 10 yr and produced dramatic results, which paved the way for a much deeper appreciation of the importance and evolution of hydrovolcanism – volcanism resulting from the interaction of magma or lava with external water. Some variations of these experiments demonstrated the potential for dynamic interaction of magma with wet sediments and produced the experimental equivalent of peperite. It is these experiments that are the subject of this paper.

While the experiments described below give some basis for understanding of peperite formation (Kokelaar, 1982; Busby-Spera and White, 1987; Brooks, 1995; White, 1996), a theoretical understanding is quite important to analyzing field observations. The theory is important because the quenching of magma during contact with water or wet sediments is really quite complex, and interpretations should fall within the realm of theoretical possibility. For this reason I address some phenomenological considerations before describing the experiments.

2. Phenomenology of wet sediment/magma interaction

Because the thermodynamic behavior of water is so well known from the steam-locomotion era, many volcanological studies have addressed the problem from a rather simplistic approach by direct applications of the First Law of Thermodynamics. While this approach does provide some limiting conditions, it completely ignores the complex issues concerning multi-phase fluid mechanics. Fluid mechanics place further constraints on the application of thermodynamics to this problem, as described by Delaney (1982) and Wohletz (1986). Such physical considerations are embodied in the concept of *fuel–coolant interaction* (FCI; Buchanan and Dullforce, 1973; Buchanan, 1974),

a field of study concerning the interaction of two fluids for which the temperature of one (fuel) is above the vaporization temperature of the other (coolant), more recently termed *molten fuel–coolant interaction* or MFCI by Zimanowski et al. (1997). For more reading on these considerations, refer to Wohletz et al. (1995), Zimanowski et al. (1991), and Zimanowski (1998).

There are important thermodynamic constraints for the phenomenology of wet sediment/magma interaction. These include the temperature and heat content of the wet sediments and magma and the rate of heat transfer between them. The amount of heat energy that is gained by the wet sediments is limited by the temperature of thermal equilibrium between the two, that is, the wet sediments can never gain more heat energy than the magma loses during their interaction. This thermal equilibrium is expressed as a function of the water/magma mass ratio, $R = m_w/m_m$. For saturated sediments or impure coolants (White, 1996), sediment particles and impurities act as heat sinks, and the mass ratio, denoted by R_s, is given as:

$$R_s = \frac{m_s}{m_m}, \tag{1}$$

where m_s is the sediment mass including pore water and m_m is the magma mass. In these situations the water/magma mass ratio is:

$$R = x_w R_s, \tag{2}$$

where x_w is the sediment water mass fraction. Using cgs units for density, the following equations can be derived, starting with an expression for x_w:

$$x_w = \frac{S\phi}{\rho_s'}. \tag{3}$$

In Eq. 3 S is the sediment saturation (the volume fraction of pores filled by water), ϕ is the sediment porosity, and ρ_s' is the sediment *bulk density*. From Eqs. 2 and 3 R may be approximated as:

$$R \cong \left(\frac{S\phi}{\rho_m}\right)\frac{V_s'}{V_m}, \tag{4}$$

where V_s' is the sediment *bulk volume* (including pore space) and ρ_m accounts for magma composition by its density (cgs units). For peperites the mass of sediments involved in their formation can be calculated. Using values for S and ϕ appropriate for the sediments involved by defining the term $S\psi \equiv S\phi/(1-\phi)$, one may determine a value for R_s by estimating the volumes of sediment and magma fragments in the peperite, V_s and V_m respectively, and measuring their respective particle densities, ρ_s and ρ_m (cgs units):

$$R_s = \left(\frac{\rho_s + S\psi}{\rho_m}\right)\frac{V_s}{V_m}. \tag{5}$$

For a simple estimate of thermal equilibrium for which there is no phase change, one may apply energy conservation for heat exchange:

$$m_s C_s(T_e - T_s) + m_m C_m(T_e - T_m) = 0, \tag{6}$$

where C is the constant volume heat capacity, T is temperature, and the subscripts e, s, and m indicate equilibrium, sediment, and magma, respectively. The heat capacity of the wet sediment, C_s, can be approximated (e.g. Buntebarth and Schopper, 1998) as:

$$C_s = x_w C_w + (1-x_w)C_s', \tag{7}$$

where C_w and C_s' denote the constant volume heat capacities of water and solid constituents, respectively. By using the mass ratio, R_s, given in Eq. 1 or 5, the thermal equilibrium limit becomes:

$$T_e \frac{R_s C_s T_s + C_m T_m}{R_s C_s + C_m}. \tag{8}$$

For a typical magma contacting 298 K water-saturated sediments, C_m and C_r are $\sim 25\%$ of C_w and T_e decreases with R_s, as shown in Fig. 1. It is evident that for magma interacting with wet sediments, T_e can exceed critical temperature [647 K (pure) to 720 K (5 wt% dissolved solids)] where $R_s < 1.0$ (basalt) and $R_s < 0.5$ (rhyolite). Where critical temperature is exceeded during interaction
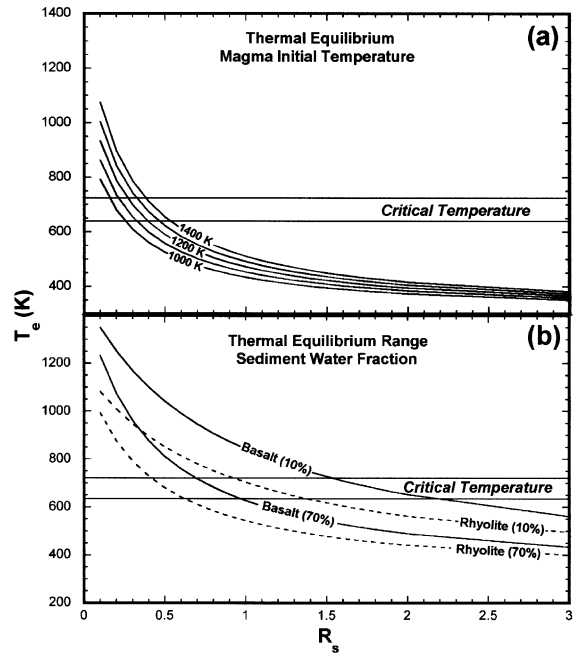

Fig. 1. Thermal equilibrium (T_e) is the maximum possible temperature water can reach during interaction with magma and is shown as a function of R_s (sediment/magma mass ratio). This example is for cases where the initial temperature of water and sediments is 298 K and the magma has typical values of heat capacity about 25% that of water. The critical temperature is shown as a range reflecting the effect of dissolved solids. (a) T_e is shown for several different initial magma temperatures interacting with water (100% volume fraction in sediments). (b) For basalt (solid curve; 1473 K) and rhyolite (dashed curve; 1173 K) interacting with wet sediments, T_e is shown as a function of sediment water volume fraction for which 10 and 70% bound a range centered on 40%, representing a porous, fully saturated sandstone, $x_w \cong 0.2$.

prior to explosive expansion, supercritical pressures will be created.

Thermal equilibrium is probably never reached during the time span of interaction because of the insulating property of a vapor film that rapidly forms at the magma–sediment interface. Because of its relatively low thermal conductivity, a vapor film can greatly decrease the rate of heat transfer from the magma to the wet sediments, allowing gradual quenching. With gradual quenching, the film slowly heats water in the sediments near the magma at a rate balanced by the heat transfer away from it by the convective movement of

pore water. However, such passive quenching is not always the case. Consider the hypothetical instantaneous interface temperature, T_i, attained by the initial contact of water with magma; it can be estimated by:

$$T_i = \frac{T_m(\alpha_m/\sqrt{\kappa_m}) + T_w(\alpha_w/\sqrt{\kappa_w})}{(\alpha_m/\sqrt{\kappa_m}) + (\alpha_w/\sqrt{\kappa_w})}. \qquad (9)$$

where α and κ are thermal conductivity and diffusivity, respectively, and subscripts m and w refer to magma and water, respectively. For the contact of a typical basalt magma with pure water, T_i approaches 1000 K. Because of the rapidity of heat exchange, water may exist in the metastable state of superheat in which it is a liquid well above its vaporization temperature. A consequence of this superheated state is that it continues to absorb heat at a high rate, reaching temperatures well in excess of its spontaneous nucleation temperature, experimentally measured at about 570 K (Reid, 1976). With temperatures approaching the critical temperature (647 K) the likelihood of vaporization by homogeneous nucleation increases to a point where a vapor film is instantly created. A vapor film formed this way rapidly expands and is highly unstable – that is, it can expand well beyond the thickness required for thermodynamic equilibrium. In doing so the vapor becomes supercooled, leading to its spontaneous condensation. The condensation then leads to a rapid collapse such that liquid water impacts the magma surface with a finite amount of kinetic energy, leading to a second spontaneous vaporization event. This cyclic vapor film growth and collapse is repeated continuously, typically with a frequency of up to 1 kHz (analogous to the *Leidenfrost* phenomena of a drop of water vibrating on a hot metal surface). Vapor film instability can generate enough kinetic energy to distort the interface between the magma and wet sediments as well cause failure of the host sediments. In some cases, film collapse can lead to jets of water-saturated sediment that actually penetrate the magma surface (White, 1996). In addition, the rapid heat loss from the magma by this continued vapor film instability leads to magma quenching and possible

granulation. With these interface phenomena, the magma gradually gets increasingly fragmented, leading to higher surface areas for heat transfer and larger volumes of superheated water and vapor.

The above system of hot magma, wet sediments, and an interface consisting of fragmented magma, superheated water, and steam can evolve in several fashions, depending upon the balance of rates of heat transfer from the magma and convective cooling by the wet sediments. If convective cooling by the sediments matches the heat transfer from the magma, the system can stabilize, forming a mixture of quenched magma and sediments. Alternatively, if the wet sediments cannot convect heat away from the growing interface fast enough, the heat transfer can grow exponentially and reach explosive rates for which the vapor film volume and pressure become too large for the enclosing sediments to contain. This situation leads to a *thermohydraulic explosion* (Büttner and Zimanowski, 1998) whose thermodynamic work is expended mainly in further magma fragmentation, seismic wave propagation, and vapor expansion, which accelerates sediment, and magma particles in directions of least resistance. For subsurface situations, fragment acceleration may occur along bedding planes, fractures, or even into the magma body itself, forming breccia dikes in the sediments as well as in the magma by a mechanism analogous to hydrofracture (Heiken et al., 1988). If the dikes penetrate the surface, a hydrovolcanic (phreatomagmatic) eruption will occur.

How the interaction of magma with water or water-saturated sediments leads to explosive phenomena is a problem that has been pondered by volcanologists for years. Wohletz et al. (1995) considered both theory and experimental evidence (Wohletz and McQueen, 1984; Wohletz, 1986) to conclude that in a general sense R is perhaps the most important controlling factor. For low values of wet sediment/magma interaction ($R_s < 0.1$) there is not enough water to produce the vapor expansion work required for an explosion. For high values ($R_s > 1.0$) there is enough water to form a convective system that balances heat transfer, so that it never grows to explosive rates. But in-between these two values, thermohydraulic ex-
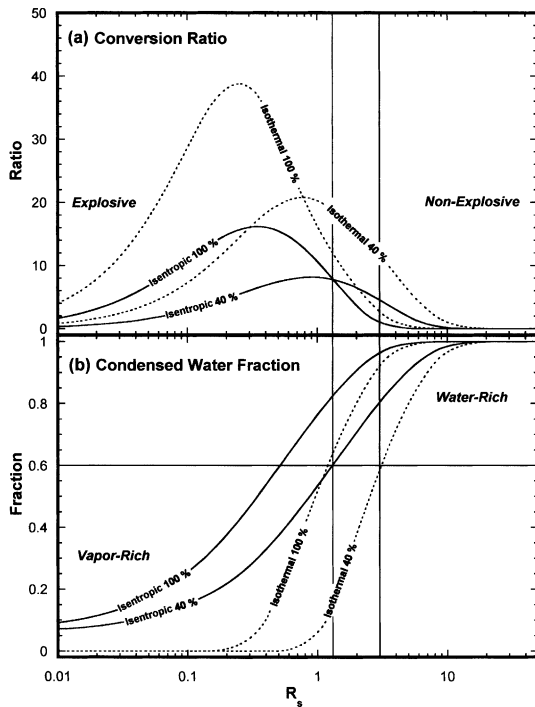
rated sediments (40% porosity, 100% saturated, 40% volume saturation, $x_w \cong 0.2$) compared to those for pure water/magma interaction (100% saturation by volume). Both *isentropic* (steam separates from fragmented magma) and *pseudo-isothermal* (steam and magma fragments remain at the same temperature, denoted in figures as *isothermal*) expansions are calculated. Note that compared to pure water/magma interactions, sediment/magma interactions have lower conversion ratios (less energetic) with optimum conversions near R_s values of 1.0. Fig. 2 also shows the fraction of vaporized water that condenses back to liquid during expansion. For interactions at low R_s values, most of the water remains in the vapor state after expansion, leading to the likelihood of explosive behavior. In contrast for R_s values

Fig. 2. Conversion ratio (a) and condensed water fraction (b) vs. the sediment/magma mass ratio, R_s (solid curves are isentropic values and dashed curves are pseudo-isothermal values). Note that in this figure and following ones, pseudo-isothermal expansions are simply labeled *isothermal*. Conversion ratios are calculated as the percentage of the magma's heat energy that is converted to thermodynamic work during interaction with water. This plot shows results for a basaltic magma at 1473 K interacting with water at 298 K (solid curves, 100% water by volume) compared with those for water-saturated sediments (dashed curves; 40% water by volume; $x_w \cong 0.2$). The condensed water fraction represents the fraction of interacting water that after expansion condenses to a liquid state. For water-saturated sediment interactions having $R_s > 1.3$ (isentropic) to 3 (pseudo-isothermal), a dominant fraction (>0.6) of vaporized water will condense to liquid during expansion to ambient pressures, and wet sediments have the ability to convectively carry heat from the magma, behaving as fluid substances rather than explosive vapor-rich ones. Using this criterion, an arbitrary region, separating explosive from non-explosive behavior, may be drawn over the range $1.3 \le R_s \le 3.0$.

plosion is possible. In Fig. 2 conversion ratios (the fraction of magma heat converted to thermodynamic work), calculated by the method described by Wohletz (1986), are shown as a measure of how much mechanical energy is released by the interaction of a basaltic magma with water-satu-
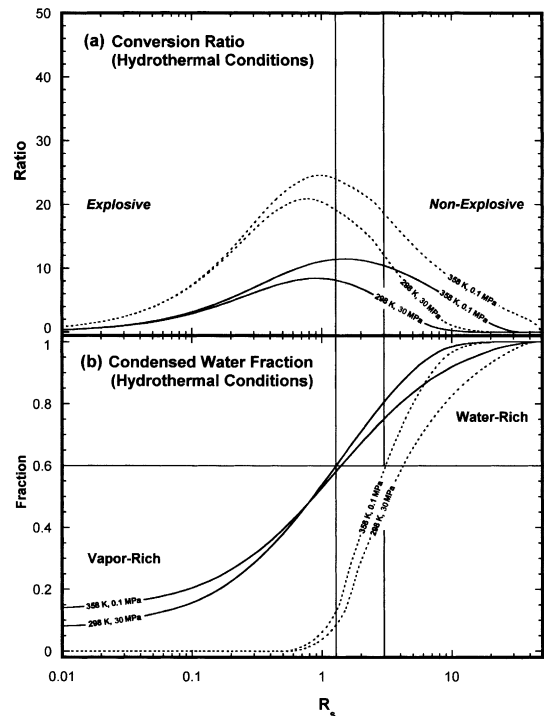

Fig. 3. Plots of conversion ratio (a) and condensed water fraction (b) vs. sediment/magma interaction ratio, R_s, for hydrothermal conditions of elevated pore water temperature (358 K) and elevated hydrostatic pressure (30.0 MPa). These curves are for a sediment containing 40% by volume water (40% porosity; 100% saturated; $x_w \cong 0.2$). The solid curves are for isentropic expansion and dashed curves are for isothermal expansion.

> 3.0 (wet sediments), a dominant portion of the steam formed condenses during expansion leaving the system as a fluid and particle system. This latter behavior allows convective heat transfer that promotes passive cooling, not likely to be explosive. Wet sediment/magma interaction may also occur at depths below the Earth's surface where hydrothermal systems of elevated temperature and pressure occur. Fig. 3 shows that for situations where sediment pore water is at elevated temperatures (e.g. 358 K) a slightly greater fraction of the magma's thermal energy is converted to thermodynamic work and optimum peaks occur at slightly higher values of R_s when compared to values shown in Fig. 2; however, elevated hydrostatic pressure (e.g. 30 MPa) does not have much effect. Still, conversion ratios at high hydrostatic pressure in excess of critical pressure are great enough that such interactions could be explosive.

In order to better illustrate the above calculations, Fig. 4 depicts water phase diagrams illustrating pressure–temperature–volume–entropy (P–T–V–S) relationships for theoretical initial equilibrium and final states. Both isentropic (Fig. 4a) and pseudo-isothermal (Fig. 4b and c) paths are shown. By comparison to phase diagrams presented by Kieffer and Delany (1979), one can see that isentropic expansion follows isentropes (Fig. 4a). In contrast, pseudo-isothermal expansion takes the vapor and magma fragment

mixture along a path intermediate to that for isentropic and pure isothermal expansions. Peperite formation likely involves isentropic expansions for pore water heated at a distance from the magma, but pseudo-isothermal expansion may take place close to the magma contact where hot fragments are mingled with wet sediment.

The phase diagrams of Fig. 4 also illustrate an important fact that experimental studies confirm: the critical point of water is not necessarily a limiting factor in vapor explosions. It has been com-
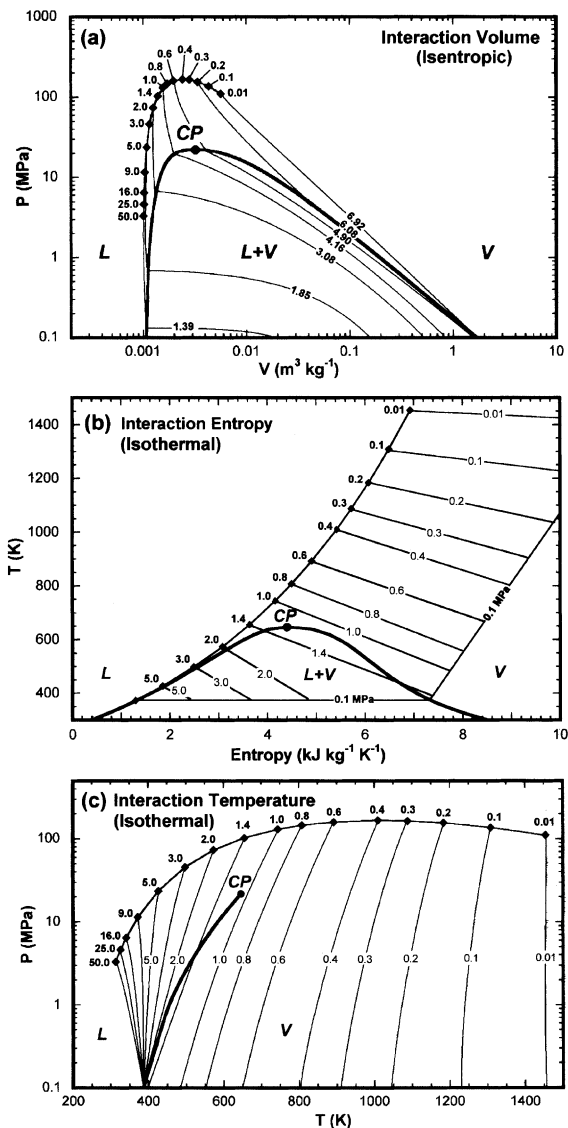

Fig. 4. Phase diagrams illustrating calculations of wet sediment/magma interaction, using the method of Wohletz (1986). Labeled points (diamonds) are the theoretical initial equilibrium conditions for interactions of various R_s (from 0.01 to 50.0; $x_w \cong 0.2$), calculated by the method of Wohletz (1986). The critical point (CP), liquid (L), vapor (V), and liquid plus vapor two-phase (L+V) regions are shown. (a) A P–V diagram shows expansion volumes and release isentropes (kJ kg^{-1} K^{-1}) followed during isentropic expansion of vapor. For all interactions, water expands into the two-phase region. (b) A T–S diagram for pseudo-isothermal expansion shows the increase in entropy as water stays in thermal equilibrium with magma fragments. For $R_s < 1.3$ water expands into the vapor field. (c) A P–T diagram shows the variation in water temperature during pseudo-isothermal expansion. For more thermodynamic details for these diagrams see Kieffer and Delany (1979).
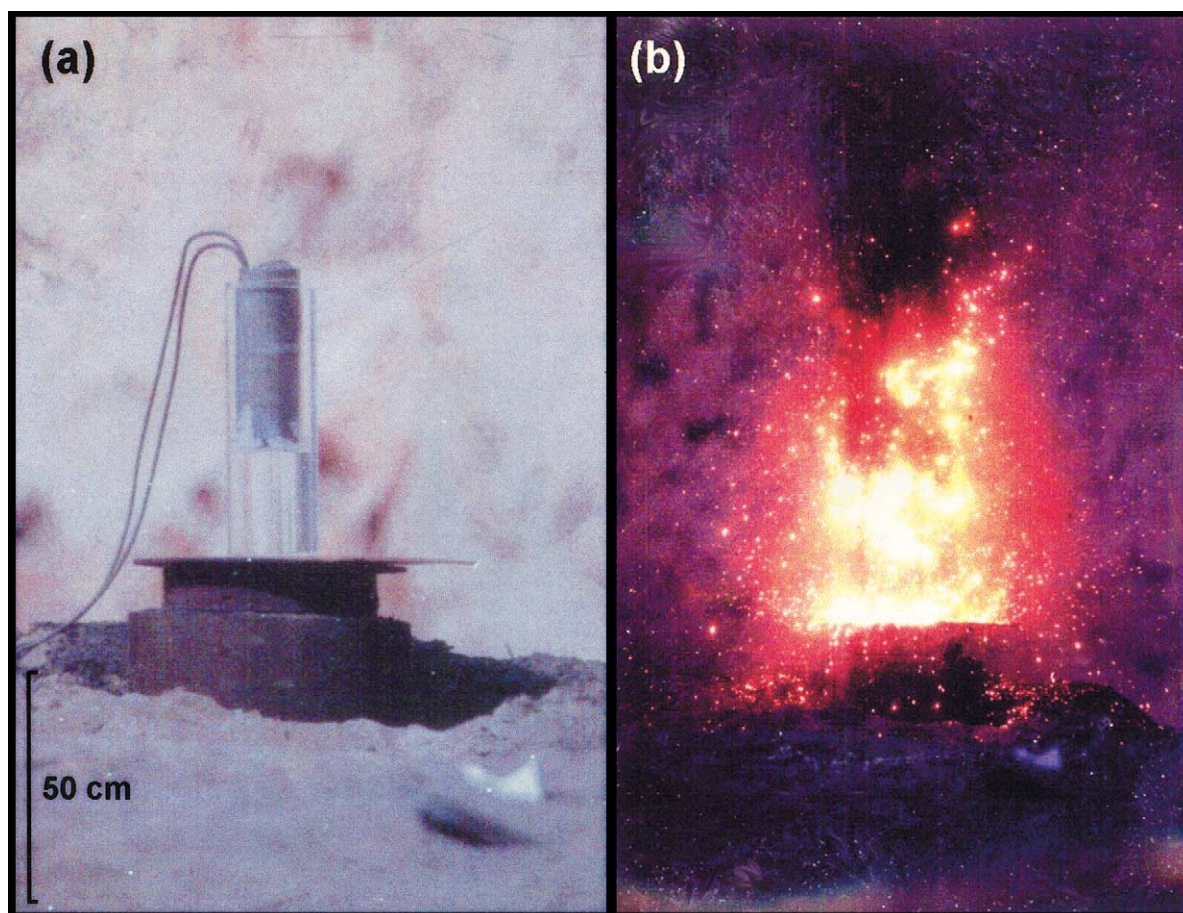
Fig. 5. Photographs depict the setup (a) and progress (b) of an experiment designed to visually assess the nature of the contact between molten thermite and water. The setup consisted of a 15-cm-diameter by 60-cm-long Plexiglas cylinder. Thermite is supported by an aluminum disk about half-way up the cylinder, and the bottom of the cylinder is filled with water. High current wires extend into the thermite to initiate its melting. When the thermite melted from the top all the way down and through the aluminum partition, interaction began. The right photo shows a bright, incandescent lobe of molten thermite penetrating down into the water. Higher in the cylinder, dark areas show clots of quenched (dark) thermite. The interaction lasted nearly 1 min during which the molten thermite was fragmented and ejected in a cloud of steam. Ejecta followed ballistic trajectories in a Strombolian-type eruption.

monly assumed by volcanologists that interactions occurring at confining pressures above the critical point of water (22 MPa) cannot result in explosions, because water exists as a supercritical fluid for which there is no liquid–vapor phase boundary. Considering the thermodynamic paths illustrated in Fig. 4 where interactions are nearly an order of magnitude in excess of critical pressure, release of the interaction pressure involves a specific volume increase, especially for pseudo-iso-

thermal expansion. This volume change occurs at a rate determined by local sound speeds discussed by Kieffer and Delany (1979). The presence of other pressure perturbations, such as those caused by seismicity, host media failure, and the vapor film dynamics, discussed above, adds to the likelihood that expansion will lead to thermohydraulic explosion. The factors governing thermohydraulic explosions are complex (Zimanowski et al., 1997), and I will not pursue them

here, but I do wish to stress the point that magma–wet sediment interactions beneath the Earth's surface or in submarine environments where hydrostatic pressure is greater than critical pressure may in certain circumstances be explosive.

Overall, when one considers geological environments where there is clear evidence of the interaction of magma with water and/or wet sediments, one may perceive shortcomings in the above physical analysis. For example, White (1996) concludes that the vent environment influences the fragmentation processes, explosive efficiency, and resultant particle populations more than water/magma mass ratio. He finds that coolant impurities, including sediment particles, enhance the ability of magma to mingle with coolant but dampen the explosivity, the latter of which is supported by results shown in Figs. 2 and 3. Furthermore, it is difficult to calculate from geological information appropriate values for R_s and the actual magma fragmentation mechanism. While there are a number of fluid dynamic mechanisms proposed to explain how interaction promotes magma fragmentation (e.g. Wohletz, 1983), rapid magma quenching evident in peperite exposures indicates that magma surfaces quench prior to much interaction, thus begging a question about fluid dynamics. Zimanowski et al. (1997) have recently shown the first experimental evidence that dynamic interaction can involve a brittle mechanism. To be sure, the physical analysis presented here is overly simple to explain much about geological occurrences where there can be a multitude of external influences on how interaction proceeds. The understanding of how external controls affect the basic physical behavior described above will require careful field observation and laboratory sample examination to determine the controls of pressure, temperature, heat exchange, and fragmentation.

3. Experimental approach

Thermite produces a melt, simulating basaltic magma, by an exothermic reaction of the fine-grained aluminum ($\sim$24 wt%) with magnetite ($\sim$76 wt%) as described by Wohletz et al. (1995):

Table 1
Representative bulk chemical analyses of thermite melt debris[a]

Oxide	Blocky particle	Silicate coating	Spindle particle
SiO_2	14.3	36.6	18.6
TiO_2	2.3	1.4	1.9
Al_2O_3	11.4	34.4	42.5
FeO	57.0	17.3	23.3
MnO	1.6	1.0	1.3
MgO	6.4	3.7	5.8
CaO	2.1	1.7	1.9
Na_2O	3.1	2.0	3.2
K_2O	2.0	2.0	1.9

[a] Standardless energy dispersive spectral analyses (EDS) with total Fe expressed as FeO.

$$3Fe_3O_4 + 8Al = 9Fe + 4Al_2O_3 + \text{heat}. \qquad (10)$$

In general this thermite composition can be shown by consideration of heats of formation to yield about 1130 kJ excess heat per mole of iron oxide at 1800 K. This excess heat allows addition of quartzo-feldspathic sand to the thermite at a ratio of $\sim$1:3 to produce a silicate melt (Table 1).

The physical and thermal properties of Fe–Al thermite melt are compared with those of a typical tholeiitic basaltic melt in Table 2. Using the methods of Bottinga and Weil (1972) and Shaw (1972), which estimate viscosity of polymeric melts containing SiO_2 and Al_2O_3, viscosities in the range of about 1 to 200 Pa s are predicted for the thermite melt over a temperature range from 1500 to 1800 K; the wide range reflects suspension effects of crystallites. Indeed, petrographic inspection of quenched samples of this

Table 2
Physical and thermal properties of Fe–Al thermite and basaltic melt[a]

Properties	Fe–Al melt	Basaltic melt
Liquidus temperature	1000–2000 K	1370–1520 K
Enthalpy	3700 kJ kg^{-1}	1150 kJ kg^{-1}
Viscosity	$\sim$10^2 Pa s	10^1–10^3 Pa s
Density	3.0–4.0 Mg m^{-3}	2.5–2.7 Mg m^{-3}
Surface tension	0.5 N m^{-1}	0.35 N m^{-1}
Thermal conductivity	2.4 J m^{-1} s^{-1} K^{-1}	2.1 J m^{-1} s^{-1} K^{-1}

[a] Properties for thermite from Buxton and Benedict (1979) and for basalt from McBirney and Murase (1984).

melt reveals abundant crystallites, which indicates subliquidus melt temperatures. Accordingly, 100 Pa s is considered typical of the viscosity of the thermitic melt used in the experiments. The reader is referred to Buxton and Benedict (1979) for further discussion on the thermochemical properties of the Fe–Al thermitic reaction.

By designing experiments to make molten thermite contact water (Wohletz and McQueen, 1984) we found that the two commonly interacted in a dynamic manner with explosive production of steam and fragmented melt. Not all experimental interactions produced explosions. In some experiments, the melt contacted the water, built up pressure in the confinement vessel, and then passively quenched. However, utilizing a number of different experimental designs, Wohletz et al. (1995) found that in general the explosiveness depends largely on the mass ratio of water and melt interacting. It was in experiments where this ratio was high ($R > 5$) that passive behavior was most likely; such experiments produced the equivalent of pillow breccia.

The experiments clearly showed that during explosive interaction the melt and water intimately mingled, breaking the melt into tiny particles that produced an extremely high surface area for rapid heat transfer. This process was observed most readily in a series of experiments for which the interaction was confined in a transparent Plexiglas cylinder that allowed video documentation. One might wonder how Plexiglas with a relatively low melting temperature could confine molten ther-

mite. The answer is that the heat from the thermite vaporizes the Plexiglas surface layer, producing a thin insulating film between the thermite and the Plexiglas. Fig. 5 shows this experimental setup and some results that demonstrate that the melt can move some distance into water before quenching and explosive interaction.

Inspection of video documentation from the experiments revealed that a vapor film served to insulate the water from the melt. But pressure records show that this film is not stable – it grows and collapses repeatedly, each cycle of growth lasting a period of milliseconds or less. With each film collapse, the melt interface is distorted and gradually fragmented, such that heat transfer to water increases with time until it is so large that a vaporization wave propagates and causes nearly instantaneous flashing of relatively large volumes of water with steam pressures large enough to breach confinement. In some cases though, the vapor film never fragments enough of the melt surface to reach heat transfer rates high enough to produce an explosion.

Realizing that in nature magma does not always come in contact with a body of water, we wondered how melt would interact with sediments containing water. Would the presence of sand grains prevent explosive interaction? The easiest experimental design called for using wet sand instead of water. Four experimental designs involved burial of a thermite-containing vessel in wet sand with and without a separate water compartment (Table 3). In general, Table 3 shows

Table 3
Thermite–wet sand experiments[a]

Experiment type	R_s	Confinement	Description
1.	0.9–1.9	0.5 m water and wet sand	1–2 mm diameter melt fragments ejected in a fountain 2–3 m high for 4–5 s; Hawaiian to weak Strombolian
2.	0.6–1.3	0.5 m water and wet sand	1 cm diameter melt fragments ejected in a fountain 7–10 m high for 2.5 s using a restricted vent nozzle; strong Strombolian
3.	1.3–2.5	0.2 m water and wet sand	Strombolian burst of cm-sized melt fragments ballistically ejected 5 m high for $\sim$1 s; Surtseyan burst of $<$1 mm ejecta to 10 m high for $<$1 s; ending with lava flow
4.	0.48–0.55	0.2 m wet sand	Strombolian activity for several seconds ballistically ejected cm-sized fragments of melt 2–5 m into the air

[a] The wet sand/thermite mass ratio $R_s \cong 5$–$10R$. Experiments 3 and 4 were repeated twice.
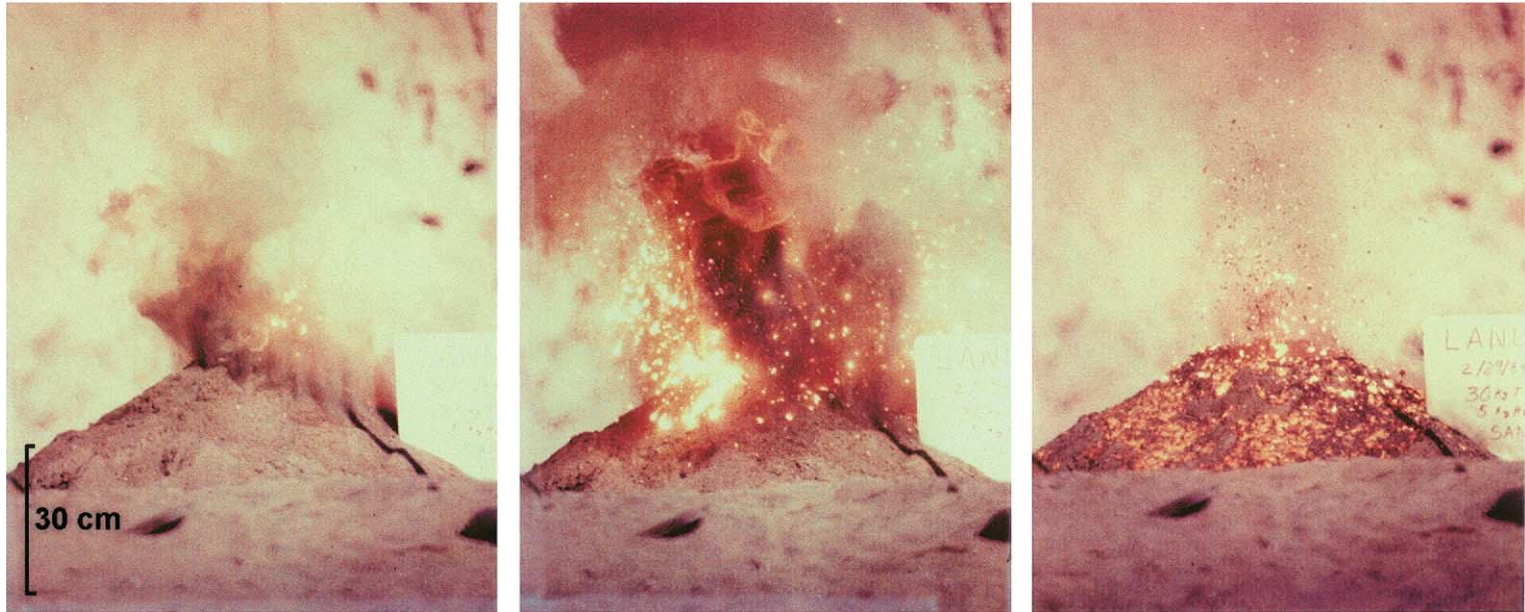
Fig. 6. A series of three photographs depicting the eruption produced by a Type 3 experimental design. The volcano edifice was constructed of sand and is about 0.5 m in diameter and 0.2 m high. Note the cm-size incandescent melt fragments following ballistic trajectories, the black finer grained melt quenched and carried up from the vent in convecting plumes while some moves downslope in a density current, and a small lava flow rivulet running downslope on the right.

results indicating that explosiveness increases with wet sand/melt mass ratio, R_s.

Fig. 6 shows the progress of a Type 3 experiment in which thermite is buried in a cone-like mound of wet sand. The thermite first interacted with a small container of water, separated from the thermite by an aluminum partition that was subsequently melted, and then with wet sand contained in the mound. This particular experiment resembled a Strombolian eruption that near its end, when the water source was depleted, formed a small lava flow. Other experiments like this one produced brief Surtseyan blasts, followed by Strombolian activity, but overall we could not tell whether the activity was related to the water body or the wet sand.

In Type 4 experiments, approximately equal volumes of wet sand and thermite ($V_s/V_m = 1.0$) were placed in the vessel shown in Fig. 7. Having $\sim 40\%$ porosity ($V_s'/V_m = 0.6$) that was ~ 50–100% saturated, the wet sand contained a mass fraction of water, $x_w \cong 0.1$–0.2, and from Eqs. 4 and 5 $R_s \cong 0.48$–0.55 ($R \cong 0.05$–0.11). The thermite was held above the wet sand by an aluminum plate. A smaller diameter steel ring, placed above the thermite, served as a nozzle to provide some pressure confinement. Above the nozzle another open cylinder directed ejecta upward. This whole assembly was situated on a platform of wet sand and stabilized in a hill of dry sand. The results of these experiments are of particular relevance to peperite formation, as discussed below.
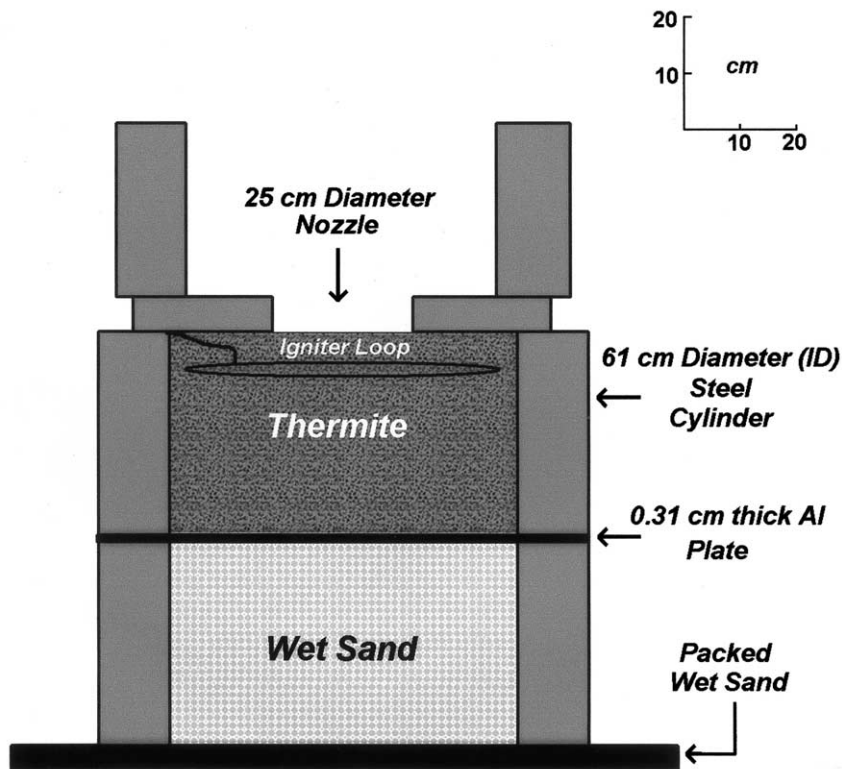

Fig. 7. Schematic illustration of the Type 4 experimental setup for the interaction of molten thermite with wet sediments (sand). This assembly was emplaced in a hill of sand with the top just at the surface of the hill. High current passed through the igniter loop initiated the thermite reaction, completely melting the thermite in less than half a minute. The melting proceeded from the top downward. When the molten thermite melted and penetrated the aluminum plate at its base, it contacted the wet sand and began the interaction.
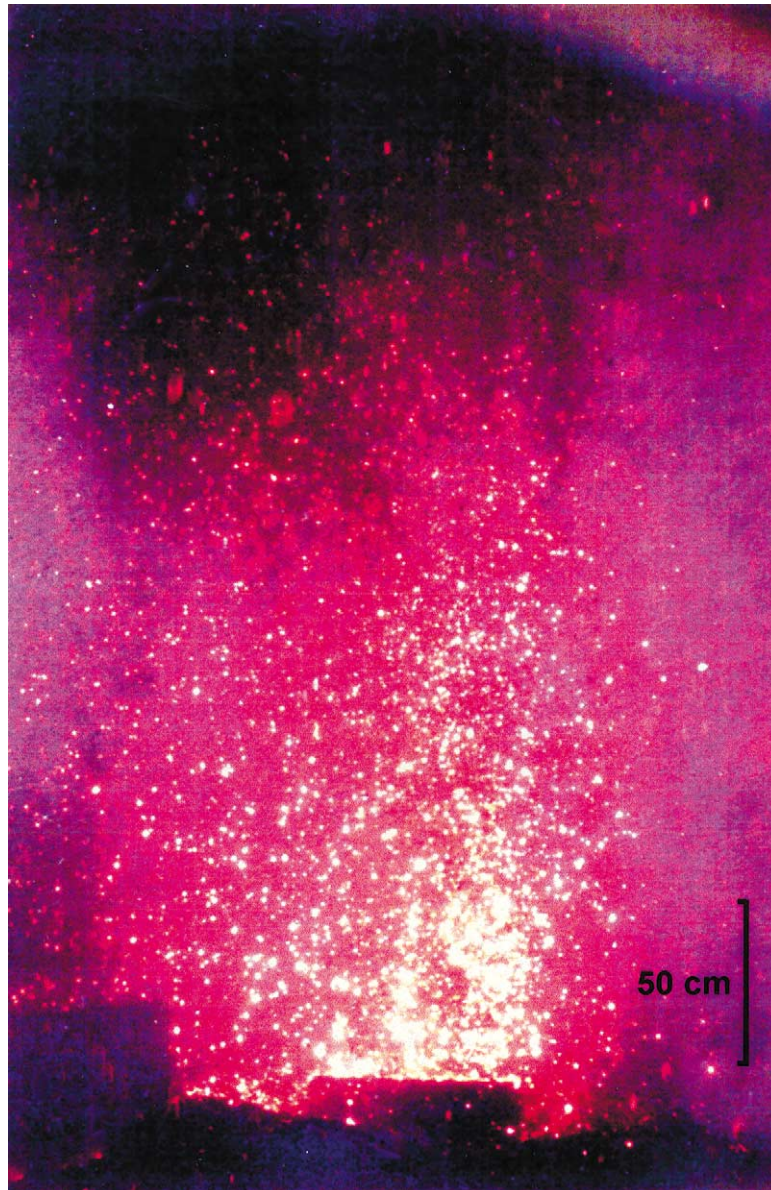
Fig. 8. Photograph of a Type 4 thermite–wet sand experiment in progress. Rapid vaporization of water in the wet sand caused fragmentation of the melt and propelled mm- and cm-sized incandescent fragments in a ballistic fountain, resembling Strombolian eruptive activity. The fountain was about 2.4 m high and rapidly fluctuated in magnitude over a duration of nearly 1 min. This photo was taken after a blast had formed a crater ring around the vessel.

4. Experimental results

The thermite melt with wet sand experiments produced dramatic evidence of the potential for explosive interaction. Fig. 8 depicts Strombolian interaction typical of Type 4 experiments. The activity lasted several seconds and was character-ized by several Strombolian bursts, reaching 2–5 m
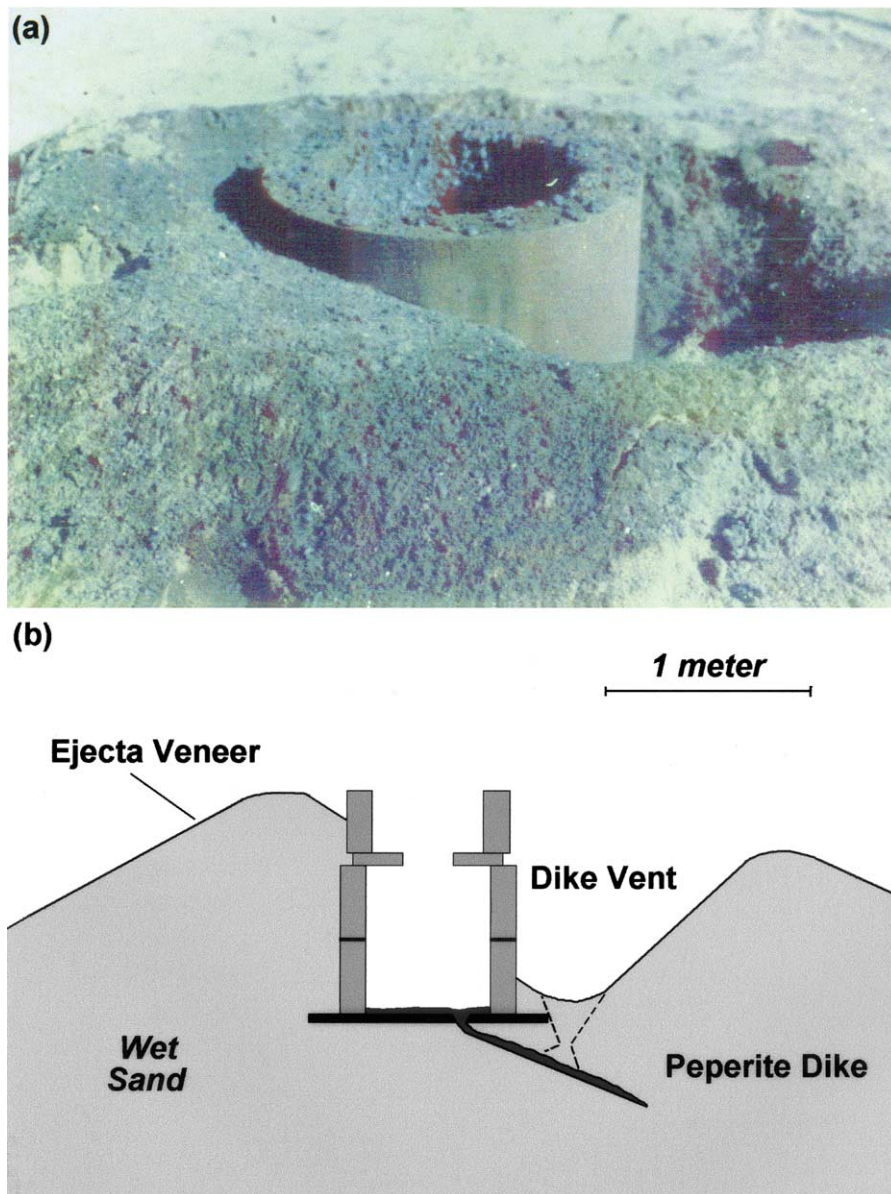
Fig. 9. (a) Photograph of Type 4 post experimental conditions showing the containment cylinder completely emptied of its contents. Note that the sand around the cylinder has been explosively excavated, forming a peripheral crater. This cratering occurred because some of the explosive ejections occurred from the base of the cylinder out into the sand. (b) A cross sectional sketch showing the relationship of the peperite dike to the experimental vessel and dike vent.

above the vent nozzle, and fragmentation of the melt into cm- and mm-sized clasts. In one Type 4 experiment, explosive interaction culminated with Surtseyan explosive activity bursting from the bottom of the cylinder, forming a crater in the sand surrounding the steel assembly (Fig. 9a).

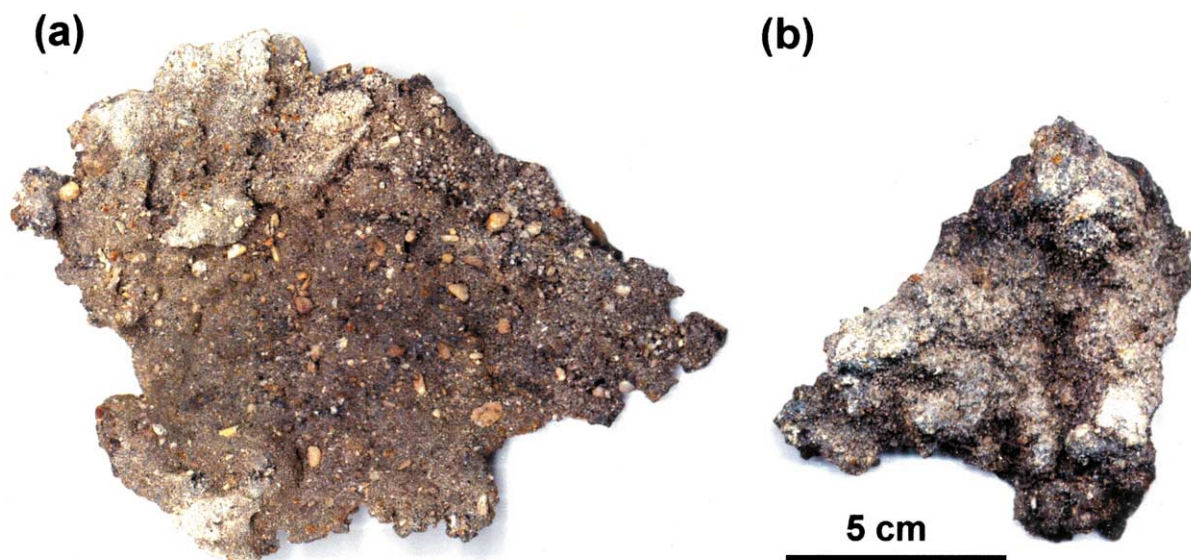Fig. 9a shows the crater and ejecta blanket on

Fig. 10. Photographs of experimental peperite samples. The dark matrix material is quenched thermite, which is thoroughly mixed with sand. Feldspar grains (a) are yellowish-brown and reach sizes up to 5 mm in length, whereas quartz grains (b) are grayish-white and are generally < 1 mm in diameter.

the sand hill surrounding the experimental assembly from the Type 4 experiment that produced culminating Surtseyan activity. The ejecta are mm-sized fragments of quenched thermite in a matrix of sand grains and fine (< 0.1 mm) thermite dust particles. The ejecta blanket extends only about 1 m outward from the vent. Fine ray-like striations visible in the ejecta are the result of alignment of coarser grains of agglomerated thermite fragments. The alignment of these striations does not point to the vent nozzle, but towards the crater that formed along side of the cylinder assembly. This observation suggests that at least a portion of the ejecta came from the venting from underneath the experimental assembly; hence, its origin is related to the peperite dike we found there.

Inspection of the Type 4 experimental assembly afterwards (Fig. 9a) revealed that most of the thermite and a similar volume of wet sand had been completely removed. Excavation into wet sand below the experimental assembly revealed that the thermite melt had penetrated completely through the wet sand compartment into the substrate, which was also wet sand. Here we found a slab-like and tuberous dike of quenched

melt, extending about 0.5 m downward and outward into the packed wet sand below the base of the experimental assembly (Fig. 9b). Apparently it was during formation of this dike that ejecta vented around the outsides of the cylinders.

Fig. 10 shows two samples of the dike. The surfaces of the dike are uneven, showing small, bulbous protrusions and wrinkles. Such surface textures are similar to the texture of *shark skin* or *elephant hide* quench textures on lava surfaces (described by Lavine and Aalto, 2002). Close inspection of the dike reveals that it is in fact composed of a quenched melt matrix enclosing sand grains. The volume fraction of quenched melt averages from 30 to 35% for these samples. The sand and quenched melt completely and intimately mingled (Fig. 11), but this mixture shows variations in the relative proportions of the constituents with clot-like quenched melt-rich and sediment-rich zones. Fig. 11 also shows that the quenched melt matrix itself appears granular, indicating that it was fragmented during intrusion and quenching. No thermal alteration or oxidation stains are visible, which indicates the rapidity of the quenching process.

Fig. 11. Close-up photographs of experimental peperite textures, showing the intimate mixing of sand grains (from 65 to 70% by volume) within the thermite magma analog. Little or no thermal alteration is visible on any of the sand grains, evidence that quenching was rapid.

5. Discussion and conclusions

From the discussion of phenomenology above, I conclude that peperite can be formed in a wide variety of geological environments where magma interacts with wet sediments. From Fig. 2 it is evident that such interaction can convert at least several percent of the magma's heat energy into thermodynamic work, which in turn is available for fragmentation of the host rock and magma, leading to mingling of the two and formation of a variety of breccia textures, including peperite. This interaction occurs over a range of wet sediment/magma mass ratios (R_s) at various confining pressures (lithostatic/hydrostatic) and initial water temperatures. Because interactions that involve R_s between 0.1 and about 1.0 have the greatest potential of being explosive (Figs. 2 and 3), characteristic peperite occurrences not easily related to explosive phenomena are likely to be formed in saturated environments where $R_s > 1$. The reader however should note that other external controls, discussed above, may be more important than R_s in controlling peperite formation.

There is some ambiguity concerning the value of R_s because one does not know a priori how much of the wet sediment and magma will interact. This value can only be estimated, as described above, from field occurrences or samples where the volume ratio of sediment fragments to magma fragments in the peperite can be measured. With estimates of sediment porosity and saturation and magma and sediment clast densities, Eq. 5 can then be applied to make an estimate of R_s, but this value will likely be only a minimum estimate because not all sediments contributing to the interaction mingle with magma fragments to form peperite. Consider a very wet, saturated sediment with 50% porosity and bulk density about two-thirds that of a basaltic magma. Applying Eqs. 2–4 one can find that its interacting bulk volume (V_s') must exceed that of magma (V_m) by nearly five times in order to achieve values of $R_s > 3$, enough to predict non-explosive peperite (Fig. 2). The peperite formed by this interaction would then have a volume ratio of sediment clasts to magma fragments greater than 3. Such situations are indeed possible, and for environments where R_s is much larger than 3 the sediments are likely to be very fluid, like quick sand or liquefied mud.

In these conditions interaction may result in the formation of globular peperite (e.g. Busby-Spera and White, 1987) or intrusive pillow breccia (e.g. Snyder and Fraser, 1963). The abundant water in these systems allows easy penetration of magma into them but they also rapidly quench the surface of the magma so that blobs of magma detach to form globular shapes like pillows (e.g. Walker, 1992) as the intrusion continues.

For the experimental results described above, only a small range of interaction ratios $R_s \cong 0.48$–0.54 was explored. During interaction of the thermite melt with wet sand in the Type 4 experimental vessel, this range of R_s resulted in mostly Strombolian-type bursts, which corresponds to an effective R of 0.5–0.1 in accordance to phenomena predicted by Wohletz and McQueen (1984). Near the end of the Type 4 experiment described above, a portion of the thermite melt intruded wet sand below the vessel. As the intrusion progressed the volume ratio of wet sand to melt increased as more melt surface area contacted wet sand. From inspections of the experimental peperite, the volume fraction of sand is about two times that of the thermite ($V_s/V_m = 2$), which from Eq. 5 corresponds to a value for R_s of about 1.8. With R_s increasing from ~ 0.5 to 1.8 as the intrusion grew, effective R values crossed the region of Surtseyan-type behavior ($0.1 \leq R \leq 1.0$; Wohletz and McQueen, 1984). When the intrusion stopped growing $R_s \cong 1.8$, which is high enough, at least theoretically, to explain why the thermite quenched to form the peperite dike.

These peperite experiments have not systematically explored the effects of varying the degree of saturation, the sediment strength, the rate at which melt is introduced to the sediments, and the confining pressure. In conclusion, however, these peperite experiments do demonstrate that the interaction of wet sediment with melt can produce vapor explosions while peperite is being formed. The experiments also show that interaction results in the intimate mingling of the melt and sediments. These results suggest that in analysis of peperite formation, the application of thermodynamic and fluid mechanic principles of FCIs as described above is appropriate.

References

Bottinga, Y.A., Weil, D.F., 1972. The viscosity of magmatic silicate liquids: a model for calculation. Am. J. Sci. 272, 438–473.

Brooks, E.R., 1995. Paleozoic fluidization, folding, and peperite formation, northern Sierra Nevada. Can. J. Earth Sci. 32, 314–324.

Buchanan, D.J., 1974. A model for fuel-coolant interactions. J. Phys. D Appl. Phys. 7, 1441–1457.

Buchanan, D.J., Dullforce, T.A., 1973. Mechanism for vapor explosions. Nature 245, 32–34.

Buntebarth, G., Schopper, R.J., 1998. Experimental and theoretical investigations on the influence of fluids, solids and interactions between them on thermal properties of porous rocks. Phys. Chem. Earth 23, 1141–1146.

Büttner, R., Zimanowski, B., 1998. Physics of thermohydraulic explosions. Phys. Rev. E 57, 5726–5729.

Busby-Spera, C.J., White, J.D.L., 1987. Variation in peperite textures associated with different host-sediment properties. Bull. Volcanol. 49, 765–775.

Buxton, L.D., Benedict, W.B., 1979. Steam explosion efficiency studies. Rep. SAND79-1399, NUREG/CR-0947. Sandia National Laboratory, Albuquerque, NM, 62 pp.

Delaney, P.T., 1982. Rapid intrusion of magma into wet rock: ground water flow due to pressure increases. J. Geophys. Res. 87, 7739–7756.

Heiken, G., Wohletz, K., Eichelberger, J., 1988. Fracture fillings and intrusive pyroclasts, Inyo Domes, California. J. Geophys. Res. 93, 4335–4350.

Kieffer, S.W., Delany, J.M., 1979. Isentropic decompression of fluids from crustal and mantle pressures. J. Geophys. Res. 84, 1611–1620.

Kokelaar, B.P., 1982. Fluidization of wet sediments during emplacement and cooling of various igneous bodies. J. Geol. Soc. Lond. 139, 21–33.

Lavine, A., Aalto, K.R., 2002. Morphology of a crater-filling lava lake margin, the Peninsula Tuff Cone, Tulelake National Wildlife Refuge, Calilfornia: implications for formation of peperite textures. J. Volcanol. Geotherm. Res. 114, 147–163.

McBirney, A.R., Murase, T., 1984. Rheological properties of magmas. Annu. Rev. Earth Planet. Sci. 12, 337–357.

McGetchin, T., Widdicombe, R., Neudecker, J., Eichelberger, J., 1976. Emplacement of the 1801 Hualalai lava flow and laboratory simulation of Mauna Loa flow. Am. Geophys. Un. Trans., Spring Mtg., Washington, DC.

Reid, R.C., 1976. Superheated liquids. Am. Sci. 64, 146–156.

Shaw, H.R., 1972. Viscosities of magmatic silicate liquids: an empirical method of prediction. Am. J. Sci. 272, 870–893.

Snyder, G.L., Fraser, G.D., 1963. Pillow Lavas. 1: Intrusive layered lava pods and pillow lavas, Unalaska Island, Alaska. U.S. Geol. Surv. Prof. Pap. 454-B, 1–23.

Walker, G.P.L., 1992. Morphometric study of pillow-size spectrum among pillow lavas. Bull. Volcanol. 54, 459–474.

White, J.D.L., 1996. Impure coolants and interaction dynamics of phreatomagmatic eruptions. J. Volcanol. Geotherm. Res. 74, 155–170.

Widdicombe, R., Wohletz, K., Neudecker, J., 1976. Experimental simulation of lava flows. Los Alamos National Laboratory Report, LA-UR 76-1577. Los Alamos National Laboratory, Los Alamos, NM, pp. 1–35.

Wohletz, K.H., 1983. Mechanisms of hydrovolcanic pyroclast formation: size, scanning electron microscopy, and experimental studies. J. Volcanol. Geotherm. Res. 17, 31–63.

Wohletz, K.H., 1986. Explosive magma-water interactions: thermodynamics, explosion mechanisms, and field studies. Bull. Volcanol. 48, 245–264.

Wohletz, K.H., McQueen R.G., 1984. Experimental studies of hydromagmatic volcanism. In: Explosive Volcanism: Inception, Evolution, and Hazards. Studies in Geophysics. National Academy Press, Washington, DC, pp. 158–169.

Wohletz, K.H., McQueen, R.G., Morrissey, M., 1995. Analysis of fuel-coolant interaction experimental analogs of hydrovolcanism. In: Intense Multiphase Interactions (Theofanous, T.G., Akiyama, M., Eds.), Proceedings of US (NSF) Japan (JSPS) Joint Seminar, Santa Barbara, CA, June 8–13, 1995, pp. 287–317.

Zimanowski, B., 1998. Phreatomagmatic explosions. Dev. Volcanol. 4, 25–54.

Zimanowski, B., Büttner, R., Lorenz, V., Häfele, H.-G., 1997. Fragmentation of basaltic melt in the course of explosive volcanism. J. Geophys. Res. 107, 803–814.

Zimanowski, B., Büttner, R., Nestler, J., 1997. Brittle reaction of a high-temperature ion melt. Europhys. Lett. 38, 285–289.

Zimanowski, B., Fröhlich, G., Lorenz, V., 1991. Quantitative experiments on phreatomagmatic explosions. J. Volcanol. Geotherm. Res. 48, 341–358.